



Preparation of bismuth-activated carbon and application to methylene orange removal

Heng Yan^{a,b,c,d}, Xin Jiang^{a,b,c,d}, Hongying Xia^{a,b,c,d,*}, Libo Zhang^{a,b,c,d,*}, Qi Zhang^{a,b,c,d}, Wei Zhang^{a,b,c,d}, Chunfu Xin^{a,b,c,d}, Kangqing Zeng^{a,b,c,d}

^aState Key Laboratory of Complex Nonferrous Metal Resources Clean Utilization, Kunming University of Science and Technology, Kunming 650093, Yunnan, China, emails: hyxiakust@163.com (H. Xia), zhanglibopaper@126.com (K. Zeng), 857384078@qq.com (H. Yan), 1228891587@qq.com (X. Jiang), 1396835730@qq.com (Q. Zhang), 841749982@qq.com (W. Zhang), 1057781417@qq.com (C. Xin), 2723202295@qq.com (K. Zeng)

^bYunnan Provincial Key Laboratory of Intensification Metallurgy, Kunming University of Science and Technology, Kunming 650093, Yunnan, China

^cKey Laboratory of Unconventional Metallurgy, Ministry of Education, Kunming 650093, Yunnan, China

^dFaculty of Metallurgy and Energy Engineering Kunming University of Science and Technology, Kunming 650093, Yunnan, China

Received 9 December 2020; Accepted 9 May 2021

ABSTRACT

In order to implement the concept of green development, the protection of the ecological environment is urgent. Bi-Bi₂O₃ loaded activated carbon (Bi-AC) was prepared from spent activated carbon by the method of ultrasound and microwave. The maximum methylene blue adsorption value of Bi-AC is 210 mg L⁻¹. The structure and properties of the Bi-AC were characterized by N₂ adsorption, X-ray diffraction, scanning electron microscopy, energy-dispersive X-ray spectroscopy, etc. The results indicate that Bi-AC consists of C, Bi, Bi₂O₃ with the Brunauer–Emmett–Teller of 1,040 m² g⁻¹. The methylene orange (MO) adsorption behaviors of Bi-AC and regenerated-activated carbon (R-AC) were investigated. The adsorption isotherms were studied by Langmuir isotherm, Freundlich isotherm and Temkin isotherm. The results revealed that the adsorption process of Bi-AC and R-AC followed Langmuir isotherm, the maximum adsorption capacity of Bi-AC for MO can reach 352.5 mg g⁻¹. The kinetic results revealed that the adsorption process of Bi-AC and R-AC followed pseudo-second-order. The Bi-AC could be employed as a photocatalyst for degradation of MO solution under ultraviolet (UV) light and visible light irradiation due to it having Bi₂O₃. The removal efficiency of MO solution was 94.9% under UV light irradiation. Moreover, the Bi-AC displayed excellent reusability. The results indicate that Bi-AC could be used as adsorbent-photocatalyst to remove the dyes from wastewater, which will realize the comprehensive utilization of waste resources.

Keywords: Microwave-ultrasound; Spent activated carbon; Bi-Bi₂O₃; Adsorption; Photocatalytic degradation

1. Introduction

With the rapid development of textile, plastic, leather, food and dyeing, a large quantity of dye wastewater has also been produced [1,2]. China's dye production has been

growing continuously for 9 y, which accounts about 70% of the total output of the world. China is the world's largest dye exporter which exports about 28% of total production [3,4]. The release of dyes into water resources can interfere with aquatic organisms and food webs, which also cause

* Corresponding author.

allergic dermatitis and skin irritation to the human body, some of which have been reported as carcinogens [5,6]. Owing to the urgent need for a clean and comfortable environment, it is imperative to treat dyes in wastewater with efficient and economical technology.

The removal approaches of dye wastewater mainly include physical methods, chemical methods and biological methods [7–10]. These methods have some defects such as high energy consumption, high processing conditions and secondary pollution although they have achieved certain effects. Adsorption is a simple, economical and environmentally friendly method to remove removing dye from wastewater [11,12]. Activated carbon (AC) is widely used in dye treatment due to its good pore structure, large specific surface area and excellent chemical stability. In the production of paracetamol, the production of large amounts of wastewater and dirt needs to be removed by activated carbon [13,14]. In addition, a large amount of spent activated carbon (S-AC) causes secondary pollution and wasting resources. Further treatment is essential to achieve comprehensive utilization of resources.

Photocatalysis technology as a new type of dye wastewater treatment technology which has the advantages of simple process and low cost since Fujishima and Honda [15] discovered the photocatalytic decomposition of water on TiO_2 electrode in the 1970s. It is considered to be a promising environmental protection technology that could decompose most organic matter effectively. Metal oxides have been widely used as photocatalysts for degrading wastewater. Bismuth oxide (Bi_2O_3) has been paid more attention among many photocatalysts which can absorb visible light and has the advantages of strong photo-carrier separation ability, high activity, non-toxicity, low cost. The bandgap of Bi_2O_3 is 2.8 eV which is narrower than TiO_2 and the photocatalytic performance of Bi_2O_3 is obviously stronger than the general photocatalyst under visible light [16–18]. Bi_2O_3 can be loaded on porous materials with uniform pore size such as activated carbon in order to improve

the visible-light photocatalytic reactivity and efficiency of Bi_2O_3 for the decomposition of organic pollutants [19,23].

S-AC which treated paracetamol wastewater was used as raw material in this experiment. S-AC was pretreated by ultrasonic wave, mixed with bismuth nitrate. After that, the material was roasted by microwave to get $\text{Bi-Bi}_2\text{O}_3$ loaded activated carbon (Bi-AC). The Bi-AC was characterized by scanning electron microscopy (SEM), energy-dispersive X-ray spectroscopy (EDS), X-ray diffraction (XRD), X-ray photoelectron spectroscopy (XPS), etc. to characterize the structure and properties. Methylene orange (MO) and CR were used as originic model to check the photocatalytic degradation of Bi_2O_3 under ultraviolet and visible light. Bi-AC is a new material based on adsorption-photocatalytic degradation of dye wastewater. The aim of the experiment is to explore a kind of technology to treat dye wastewater for the sustainable development of the environment.

2. Materials and methods

2.1. Chemicals

S-AC was used as raw material which collected from a paracetamol company in Liaoning Province of China. All chemicals used in this work such as $\text{Bi}(\text{NO}_3)_3 \cdot 5\text{H}_2\text{O}$, methylene blue (MB), MO, HCl, NaOH, ethanol were analytically pure (Tianjin Zhiyuan Chemical Reagent Co., Ltd., China).

2.2. Preparation of Bi-AC

As shown in Fig. 1, (1) Ultrasonic treatment: a certain amount of S-AC with distilled water was put into the beaker, then treated by ultrasonic wave equipment (Shengyuan SY 1200-T, China) for 3 h at the power of 1,200 W. The sample obtained after washing was called F-AC; (2) Dipped treatment: the washed AC was dried in an electric oven (Yiheng DHG-9003, China) at 80°C for 12 h. 100 g of F-AC was impregnated with 500 mL of 0.15 mol L^{-1}

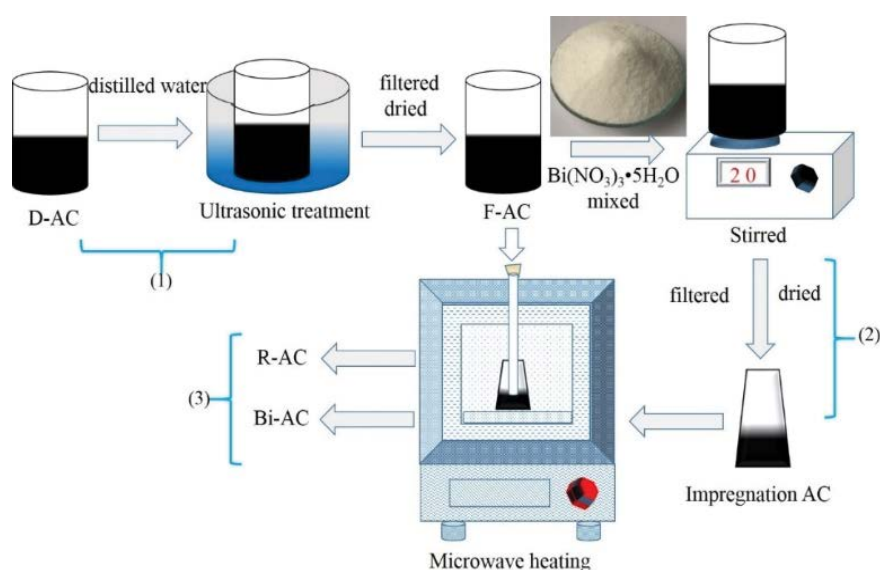


Fig. 1. Schematic diagram of the activated carbon preparation process.

Bi(NO₃)₃ solutions stirring for 12 h at 100 rpm then filtered and dried at 80°C for 12 h to obtain the impregnated AC; (3) Microwave roasted: took 15 g F-AC or impregnated AC into microwave oven (Maikewei HM-X08-16, China) at the power of 1,000 W was heated at different temperatures and time. The samples can be removed from the microwave oven until it cools to room temperature. The sample is stored in a sealed bag for further characterization and experimental studies.

2.3. Characterization of adsorbents

The adsorption capacity of Bi-AC was tested with MB using the standard testing methods of the People's Republic of China (GB/T12496.10-1999) [24]. The sample was characterized by X-ray diffraction (XRD, X'Pert Pro) which can analyze the crystal structure and the phase of the material accurately. In order to obtain the surface morphology using the SEM and EDS were used to detect the material. It was operated in a Philips XL30 ESEM-TMP SEM with an acceleration voltage of 15 kV. The Brunauer–Emmett–Teller (BET) test sample was used N₂ adsorption. The specific surface area, pore size distribution, total pore volume and nitrogen adsorption–desorption curve was calculated according to the N₂ adsorption data to obtain the pore structure of the activated carbon. XPS was carried out by a Kα + electron spectrometer (Thermo Fisher Scientific, USA) equipped with Al Kα X-ray source at 12 kV and 6 mA. The zeta potential was measured by the interpolation method using an omnidirectional multi-angle particle size and high sensitivity zeta potential analyzer.

2.4. Effects of MO adsorption

2.4.1. Adsorption isotherms

To obtain the adsorption isotherms of MO solutions onto regenerated-activated carbon (R-AC) and Bi-AC. The calculated constants of isotherm equations were applied to obtaining the properties of adsorbents. The adsorption experiments were conducted in the initial concentration of 300 mg L⁻¹ with different temperatures of 30°C–50°C. Three isotherm models were employed to evaluate the adsorption equilibrium characteristics of MO on R-AC and Bi-AC [25]. The basis of the equilibrium Freundlich isotherm is that the absorption occurs at a heterogeneous surface that energy is not distributed uniformly. This heterogeneity leads to the creation of various functional groups on the adsorbent and, consequently, promotes the formation of various mechanisms at the interaction between adsorbent and adsorbent. Models were listed in Table 1 [26,27].

2.4.2. Adsorption kinetics

The kinetic model can provide effective information about the adsorption reaction pathway. The adsorption kinetics was studied by pseudo-first-order, pseudo-second-order and intraparticle diffusion. The three adsorption kinetic models are listed in Table 2 [28,29].

The amount of adsorbed MO onto R-AC and Bi-AC over time (q_t , mg L⁻¹) and the adsorption capacity of R-AC and Bi-AC at equilibrium (q_e , mg L⁻¹) can be calculated from Eqs. (1) and (2):

Table 1
Models of adsorption isotherms

Isotherm	Equation	Parameters
Langmuir	$\frac{1}{q_e} = \frac{1}{(K_L Q_0 C_e)} + \frac{1}{Q_0}$	K_L (L mg ⁻¹) – the adsorption equilibrium constant Q_0 (mg g ⁻¹) – the maximum capacity
Freundlich	$\ln q_e = \ln K_f + \frac{1}{n} \ln C_e$	K_f – adsorption constant n – adsorption constant
Temkin	$q_e = A + B \ln C_e$	A and B – constant

Table 2
Models of adsorption kinetic

Kinetic models	Equation	Parameters
Pseudo-first-order	$\ln(q_e - q_t) = \ln(q_e) - \frac{k_1}{2.302} t$	k_1 (min ⁻¹) – the adsorption rate constant
Pseudo-second-order	$\frac{t}{q_t} = \frac{1}{k_2 q_e^2} + \frac{t}{q_e}$	k_2 (g mg ⁻¹ min ⁻¹) – the equilibrium rate constant
Intraparticle diffusion	$q_t = k_{\text{dif}}(t^{1/2}) + C$	k_{dif} (mg g ⁻¹ min ^{1/2}) – the intraparticle diffusion rate constant C – constant

$$q_t = \frac{(C_0 - C_t)V}{M} \tag{1}$$

$$q_e = \frac{(C_0 - C_e)V}{M} \tag{2}$$

where C_0 (mg L^{-1}) is the initial concentration of MO, C_e (mg L^{-1}) and C_t (mg L^{-1}) are the MO concentration of equilibrium and at time t (min), respectively; V (L) is the volume of the liquid-phase and M (g) is the mass of the adsorbent.

2.5. Photocatalytic reaction

The photocatalytic activity of Bi-AC in a photocatalytic reactor was tested under ultraviolet and visible light conditions. The UV light was generated with a mercury lamp (PLS-LAM 250), visible light was generated with a xenon lamp (PLS-LAX 250) used MO solution was selected for experiments. The specific steps are as follows: 50 mg of Bi-AC is weighed into MO solution (200 mL) at the concentration of 200 mg L^{-1} and the reaction solution is stirred under dark conditions for 80 min to eliminate the influence of adsorption. The solution was extracted every 20 min and centrifuged. The absorbance of the center is measured by an ultraviolet-visible spectrophotometer (UV-Vis). The UV-Vis spectra were recorded in the range of 200–800 nm at room temperature by Shimadzu UV-2600. Eq. (3) is calculated according to the degradation rate:

$$D(\%) = \frac{C_0 - C_t}{C_0} \times 100 \tag{3}$$

where D (%) is the degradation rate of the dye, C_t (mg L^{-1}) is the concentration of the dye solution at time t (min), C_0 (mg L^{-1}) is the initial concentration of the dye.

The photocatalytic performance was examined five times in order to further study the recyclability of the Bi-AC. Bi-AC reached an adsorption saturation state, photocatalytic experiments were carried out many times to explore the removal rate of dye wastewater in each recyclable experiment.

3. Results and discussion

3.1. Preparation of adsorbents

3.1.1. Effect of roasted temperature

Experiments were carried out on R-AC and Bi-AC for different heating temperatures for 30 min. The effect of temperature from 500°C to $1,000^\circ\text{C}$ on MB adsorption is shown in Fig. 2.

As shown in Fig. 2, the maximum MB adsorption value of Bi-AC is 195 mg L^{-1} at 900°C . The MB adsorption value increases gradually from 500°C to 900°C and then tends to decrease. There are two main reasons for this phenomenon. First, when the temperature is low, the organic matter and residues in some pores of the activated carbon are desorbed

by microwave heating. Secondly, the higher temperature can lead to the pore walls destructive. The Bi_2O_3 would melt agglomerated during the heating process. The agglomerated particulate matter will block the pores of the AC, reducing the adsorption performance of the AC, leading to a downward trend in the yield. The agglomerated particles will block the pore of the activated carbon and reduce the adsorption performance of the activated carbon. This showed that the heating temperature had a great influence on its adsorption capacity [1,5].

3.1.2. Effect of heating time

The effect of heating time on the removal of the MB is shown in Fig. 3. The MB adsorption of R-AC and Bi-AC increased progressively with heating time increasing, which indicates that a large amount of organic matter in the material's pore degraded in a short-time heating process and the generated gas is favorable for dredging the pores.

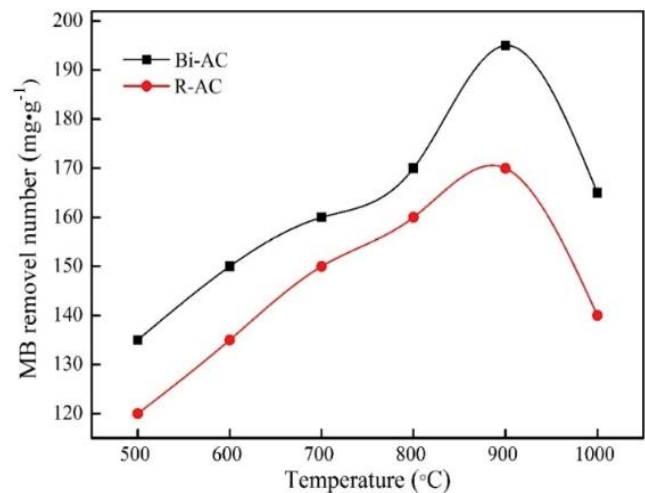


Fig. 2. Effect of roasted temperature of Bi-AC and R-AC on MB adsorption.

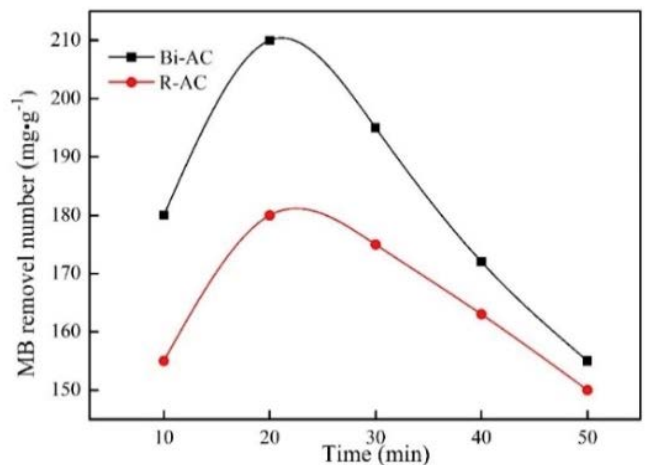


Fig. 3. Effect of heating time of Bi-AC and R-AC on MB adsorption.

However, the pore walls of the material gradually collapse and the pores were blocked. Therefore, the adsorption amount of MB decreases when the time exceeds 20 min.

The product roasted at 900°C using the heats time of 20 min can be gained a great MB adsorption value (210 mg L⁻¹) in summary.

3.2. Characterization of the adsorbents

3.2.1. BET analysis

The N₂ adsorption–desorption isotherms of S-AC, R-AC and Bi-AC are presented in Fig. 4. As shown in Fig. 4, according to the standard adsorption classification of IUPAC, activated carbon has capillary condensation and an obvious hysteresis loop, which indicate that the materials have mesopores, the curves belong to the combined types of II and IV, and the hysteresis loops had the characterization of H4. The isotherm of the two-way alternating current has a higher adsorption amount, indicating that the microporous structure increases after loading, and it has a better adsorption capacity at lower relative pressure [30,31].

The pore structure parameters are summarized in Table 3. The specific surface area of Bi-AC relative to S-AC and F-AC increased by 535.73 and 171.36 m² g⁻¹, and the average pore size decreased indicates an increase in the number of micropores. The increase in micropores of the Bi-AC can increase the amount of dye adsorbed.

3.2.2. XRD analysis

The crystal structure and the phase analysis of Bi-AC are observed by XRD accurately. The XRD patterns of the

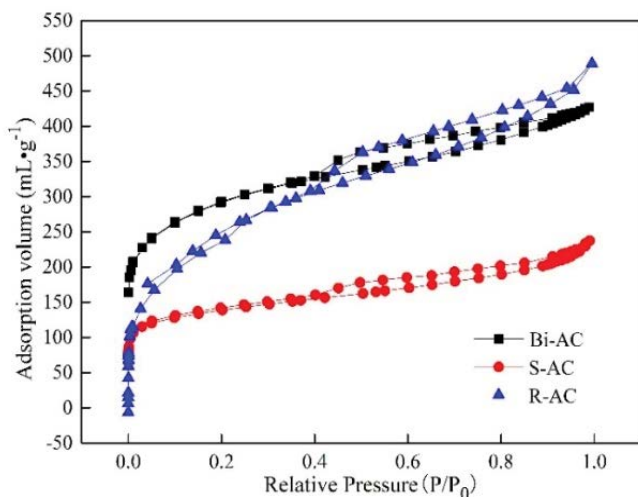


Fig. 4. Isotherm linear plots.

Table 3
Pore structure parameters of S-AC, R-AC and Bi-AC

Material	S-AC	R-AC	Bi-AC
S _{BET} (m ² g ⁻¹)	504.63	869.00	1,040.36
Average pore size (nm)	2.91	1.40	2.54
Total pore volume (cm ³ g ⁻¹)	0.99	0.68	0.98

as-prepared samples is shown in Fig. 5. It can be found from Fig. 5 that the Bi-AC consists of C, Bi and Bi₂O₃. Bi-AC indicates a substantial degree of crystallinity owing to its strong and sharp diffraction peaks [32]. The sharp diffraction peak of Bi-AC near 2θ = 28.1° corresponds to the (2 0 1) plane showed the preferred orientation of the particles indicating the presence of tetragonal β-Bi₂O₃ in accordance with the standard card of Bi₂O₃. The appearance of Bi is due to the reduction of Bi₂O₃ produced by C [33]. The activated carbon was immersed in a certain concentration of the bismuth nitrate solution and roasted under a microwave field. The bismuth nitrate precursor enters the pore or surface of the activated carbon to form Bi₂O₃ or Bi and does not destroy the pore structures. The oxide of bismuth was successfully loaded onto the surface of the activated carbon according to the XRD analysis [25,26].

3.2.3. SEM micrographs and EDS analysis

SEM and EDS of S-AC, R-AC and Bi-AC are shown in Fig. 6. The surface was rough and had impurities in Fig. 6a. Ultrasonic pretreatment and microwave regeneration, impurities removal the surface of R-AC in Fig. 6b. Furthermore, the Bi-AC consists of C, O and Bi used dipped-rotating as shown in Fig. 6c. The worm-like Bi₂O₃ was supported on the surface of Bi-AC. The result was consistent with XRD.

3.2.4. XPS analysis

XPS is used to characterize the composition content and surface chemical state of compounds in composite materials [34]. The XPS spectra of Bi-AC are shown in Fig. 7. It can be found that the Bi-AC mainly had three elements of C, O and Bi from Fig. 7a. As shown in Fig. 7b, under the separation of Bi³⁺, it could be observed that the peak at 159.4 eV was assigned to Bi 4f_{7/2}, indicating that Bi was present in a positive trivalent oxidation state; the peak

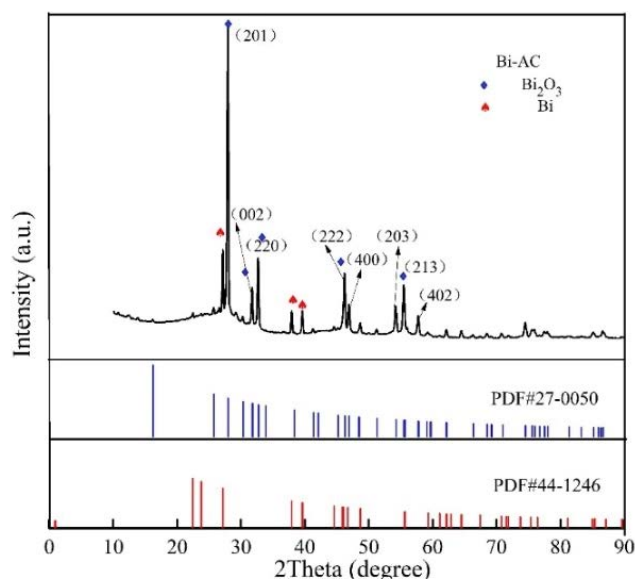


Fig. 5. XRD patterns of Bi-AC.

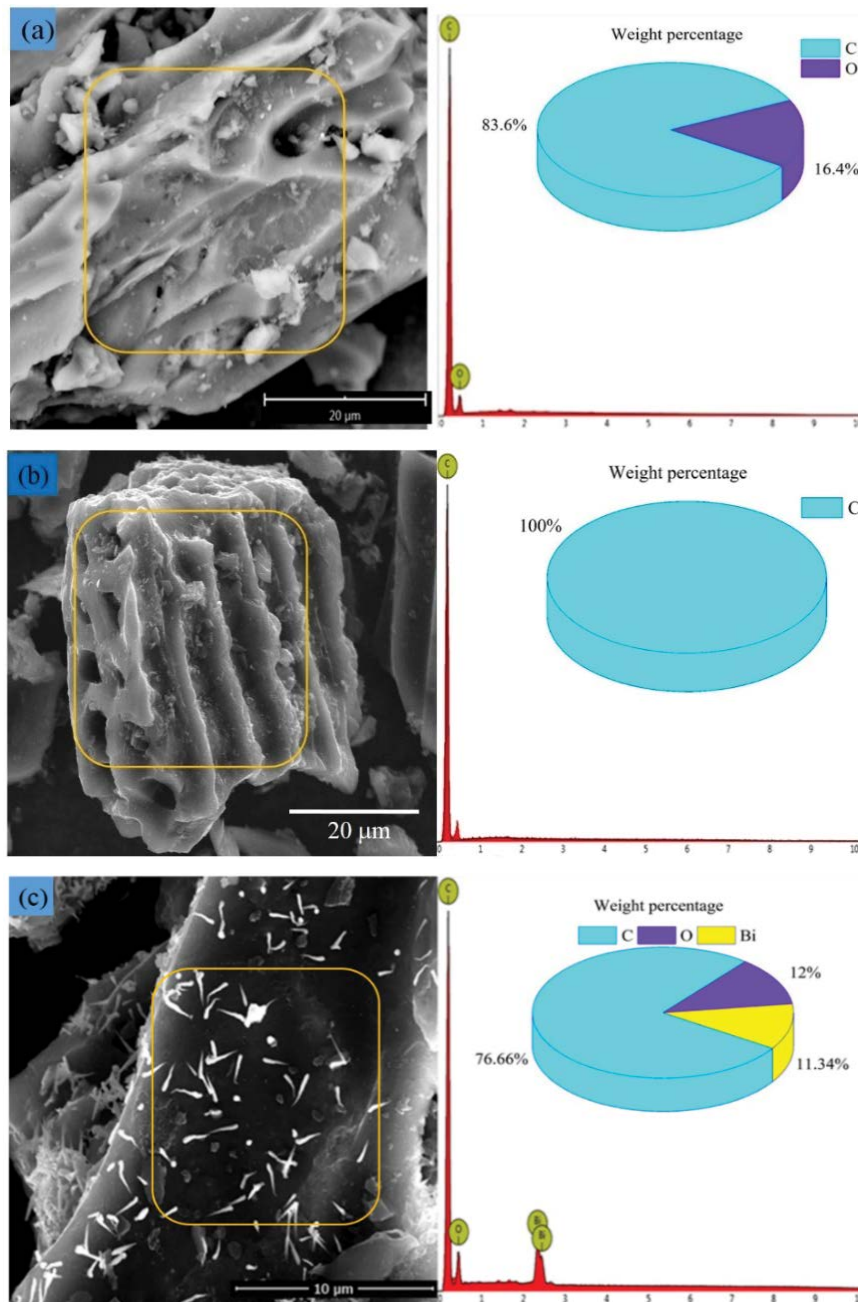


Fig. 6. SEM and EDS images of (a) S-AC, (b) R-AC and (c) Bi-AC.

at 164.7 eV was assigned to Bi $4f_{5/2}$. Compared with the binding energy of bismuth (158.7 and 163.9 eV), the binding energy of Bi in activated carbon was higher because some of the lattice oxygen in the activated carbon was replaced by carbon atoms [35,36]. C was lower than the electronegativity of O reduced the electron density on Bi [37]. Fig. 7c shows the XPS of O 1s of Bi-AC. The O 1s spectrum can be decomposed into oxygen (Bi–O) in the lattice at 533.9 eV and surface adsorbed oxygen (OH^- or CO_3^{2-} group) at 531.9 eV. Fig. 7d shows the XPS of C 1s of Bi-AC. It could be seen from the figure that the peak of C 1s could be divided into Gaussian peaks centered at

284.5 and 286 eV and the binding energy of 284.5 eV was mainly related to activated carbon. The O–C=O functional group was related to the peak at 286 eV due to the presence of carbon in the activated carbon. It could also be found that bismuth nitrate was decomposed by heating to form Bi_2O_3 which was consistent with the XRD results from the XPS results.

3.2.5. Raman analysis

Fig. 8 shows the Raman spectrum of Bi-AC and R-AC. As Fig. 8 shows, the R-AC and Bi-AC have two significant

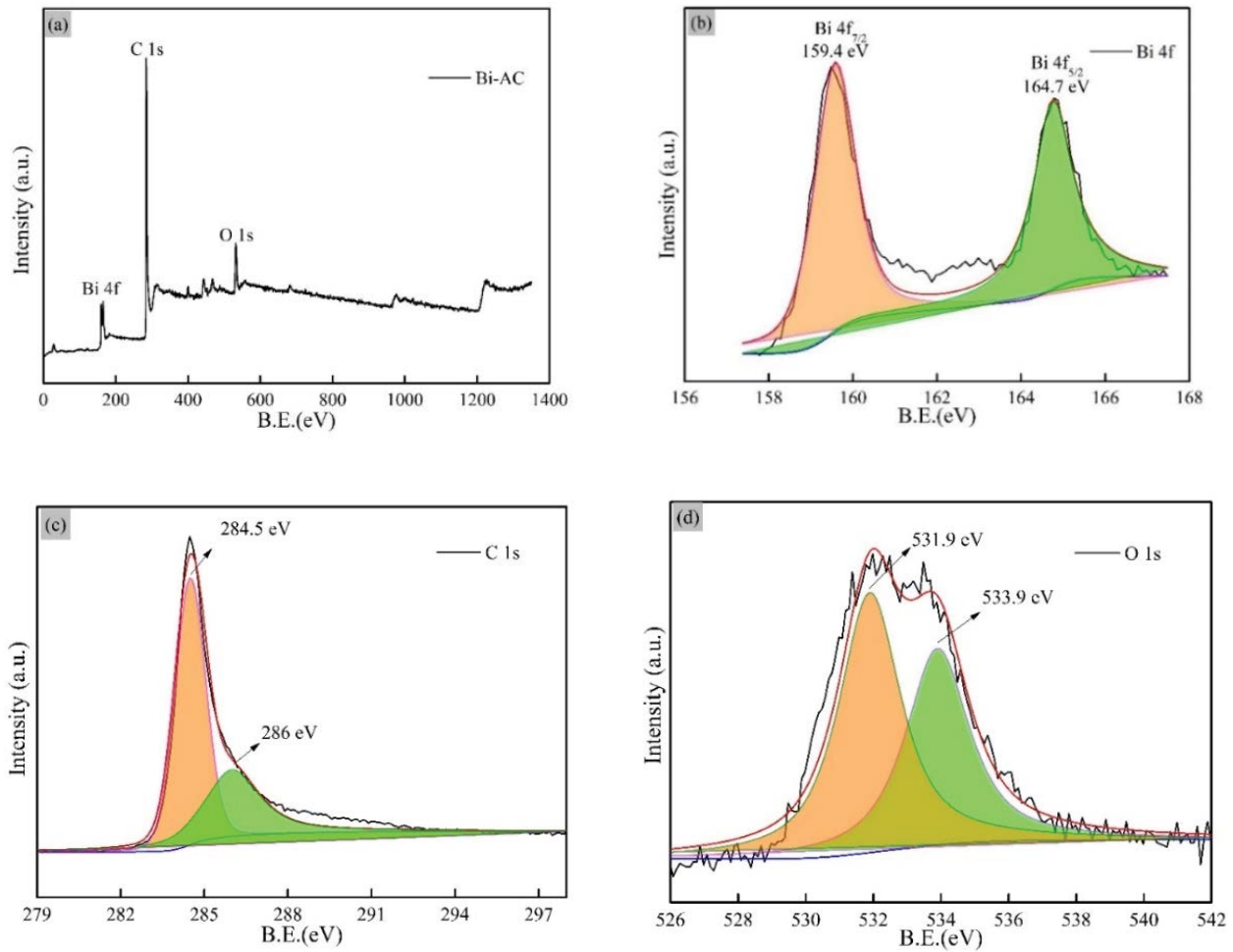


Fig. 7. XPS spectra of Bi-AC (a) survey spectrum, (b) Bi scan, (c) C scan, and (d) O scan.

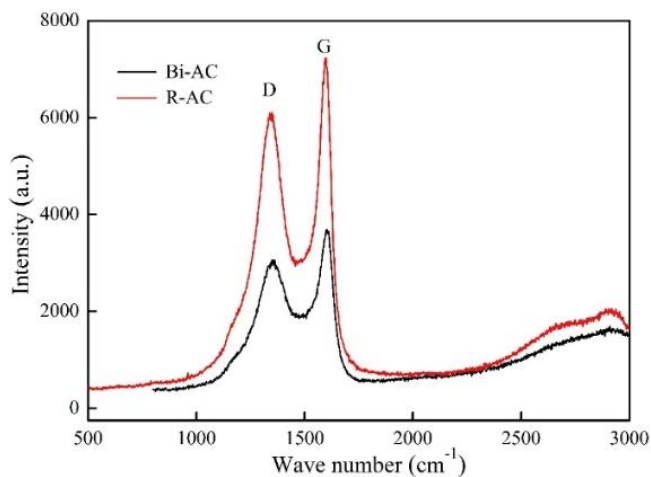


Fig. 8. Raman spectrograph of Bi-AC and R-AC.

peaks at the wavenumbers of 1,340 and 1,595 cm^{-1} which are the D peak and the G peak. The appearance of the D peak is caused by the defect of the sp^3 carbon atom in the activated carbon crystal lattice and the G peak was caused by the in-plane stretching vibration of the sp^2 hybridized

carbon atom in the two-dimensional hexagonal lattice. There was a significant shift between the D peak and the G peak for the Bi-AC. The D peak and the G peak appear at 1,350 and 1,605 cm^{-1} [38]. The peak of the D was relatively more extensive than the G peak due to some oxygen-containing functional groups have been introduced when the calcination process.

3.2.6. Zeta potential analysis

Fig. 9 shows the zeta potential of R-AC and Bi-AC. Zeta potential is the significant electrokinetic property that can quantify the potential of adsorbent surface. The zeta potential of the Bi-AC was 5.3 and the R-AC was 4.8, which indicates that the activated primary functional group of activated carbon increases after modification caused the acidic functional group was reduced, as shown in Fig. 9. A strong electrostatic attraction between the positive charge on the surface of AC and the anionic could promote the adsorption of the dye under acidic conditions. However, electrostatic repulsion occurs between the two which was not conducive to the adsorption of anionic under alkaline conditions as the amount of negative charge on the surface of AC increases.

3.3. Adsorption behavior of Bi-AC and R-AC

3.3.1. Adsorption isotherms studies

The adsorption isotherms indicates the distribution of the molecules of adsorbate between the liquid phase and solid phase when the adsorption process reached equilibrium. The adsorption isotherms were studied by Langmuir isotherm, Freundlich isotherm and Temkin isotherm. The calculated constants of isotherm equations were applied to obtaining the properties of adsorbents. The adsorption experiments were conducted in the initial concentration of 300 mg L⁻¹ with different temperatures of 30°C–50°C. The calculated parameters of MO on to Bi-AC and R-AC for three isotherm equations are listed in Table 4. According to the obtained constants, it can be found that the R² for Langmuir isotherm was satisfactory. It revealed that the adsorption process had the characteristic of monolayer adsorption and the process was uniform. The maximum adsorption capacity of Bi-AC for MO can reach 352.5 mg g⁻¹. The Langmuir isotherm for the adsorption of MO onto Bi-AC and R-AC are shown in Fig. 10.

The Langmuir isotherm model is based on the molecules, or ions, bond to certain points at the surface of the adsorbent material, and monolayer absorption occurs. Besides, no interaction occurs between absorbed molecules [26,30].

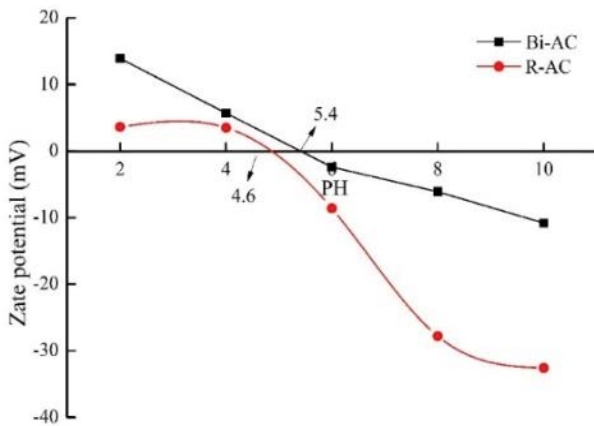


Fig. 9. Zeta potential of Bi-AC and R-AC.

3.3.2. Adsorption kinetics

The kinetic constants were essential to analyze the adsorption process and the adsorption rate can be obtained to provide the mechanism analysis of adsorbent onto the dye solution. The obtained kinetic parameters for the

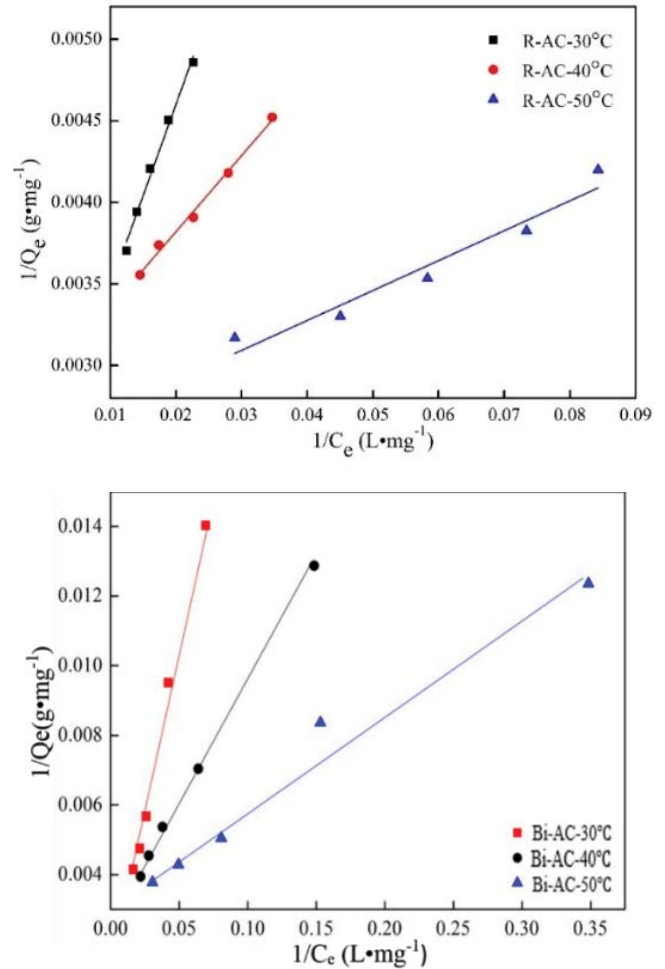


Fig. 10. Langmuir isotherm for the adsorption of MO dye onto Bi-AC and R-AC.

Table 4
Adsorption isotherm parameters calculated for the adsorption of MO onto Bi-AC and R-AC

Isotherm	Parameters	Bi-AC			R-AC		
		30°C	40°C	50°C	30°C	40°C	50°C
Langmuir	Q ₀ (mg g ⁻¹)	318.6	336.4	352.5	297	329	340
	K _L (L mg ⁻¹)	0.39	0.84	1.22	0.03	0.08	0.16
	R ²	0.994	0.999	0.973	0.987	0.982	0.931
Freundlich	1/n	0.14	0.17	0.23	0.24	0.27	0.25
	K _F	6.66	23.85	48.13	3.61	4.52	4.89
	R ²	0.992	0.964	0.972	0.950	0.919	0.849
Temkin	A (L mg ⁻¹)	266.46	95.684	11.262	199.1	228.2	262.8
	B	122.42	88.73	79.73	25.8	18.5	40.1
	R ²	0.92	0.92	0.977	0.958	0.908	0.878

adsorption of MO onto Bi-AC and R-AC are given in Table 5. It is seen, that the values of R^2 for pseudo-second-order were highest of Bi-AC and R-AC reached 0.9999 and 0.9995. It showed that the pseudo-second-order model was more applicable and reliable which can predict the experimental data [39].

For the pseudo-second-order model, the calculated adsorption capacity is slightly different from the experimental data, and the linear regression relationship is also high which indicates that the adsorption of MO by Bi-AC can be described by pseudo-second-order description and the whole adsorption process is controlled by chemical adsorption.

The pseudo-second-order model for the adsorption process of MO onto Bi-AC and R-AC is shown in Fig. 11. It can be found that the curve of t/q_t vs. t is a straight line.

3.4. Photocatalytic activity

3.4.1. Photocatalytic performance of Bi-AC

The photocatalytic activities of the Bi-AC were evaluated by monitoring the degradation of MO in an aqueous solution under visible/ultraviolet irradiation, respectively.

Table 5
Kinetic parameters obtained for the adsorption of MO onto Bi-AC and R-AC

Kinetic models	Parameters	Bi-AC	R-AC
Pseudo-first-order	k_1	0.03	0.025
	q_e	30.67	41.23
	R^2	0.9105	0.8821
Pseudo-second-order	k_2	0.00017	0.001
	q_e	363.14	427.29
	R^2	0.9999	0.9995
Intraparticle diffusion	k_{dif}	18.74	4.805
	C	167.8	404.107
	R^2	0.9613	0.9786

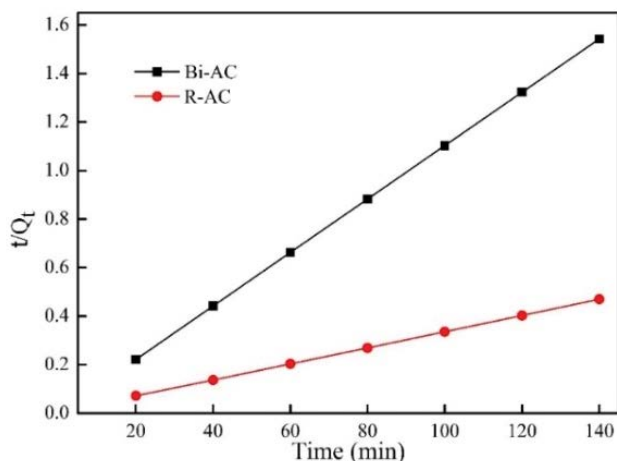


Fig. 11. The pseudo-second-order model for the adsorption process of MO onto Bi-AC and R-AC.

The best photocatalytic degradation efficiencies of Bi-AC under ultraviolet light were achieved about 94.9% for MO dye molecule; the best photocatalytic degradation efficiencies of Bi-AC under visible light were achieved about 72.5% for MO dye molecule after irradiation for 200 min as shown in Fig. 12. MO removal rate increased by 22.4% compared with visible light. Bi-AC provides a channel for the diffusion and transport of dye molecules and hydroxyl radicals due to its high specific surface area and pore volume. The dye molecules were adsorbed to the surface by activated carbon and transferred to Bi_2O_3 where photocatalysis occurs which could increase the dye removal rate.

Fig. 13 is the actual effect diagram of the above experiment. Adsorbed under dark conditions for the first 80 min, and irradiated by ultraviolet light for the next 80 min.

3.4.2. Photocatalysis mechanism

Taking the degradation of MO solution as an example, the steps are as follows: the MO dye was adsorbed on the surface of the Bi-AC at first; the MO dye molecule

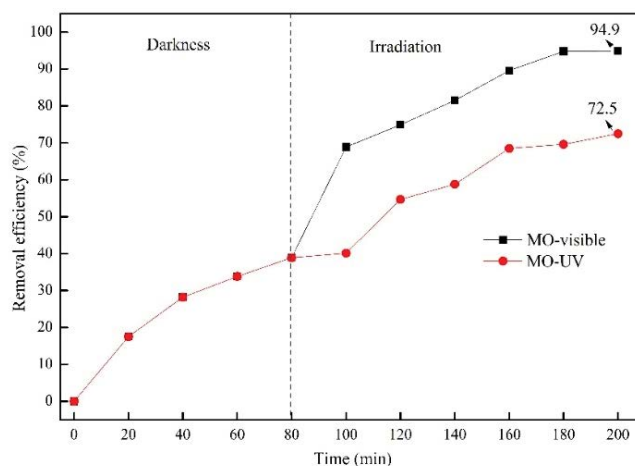


Fig. 12. The removal rate of MO under visible/ultraviolet light.

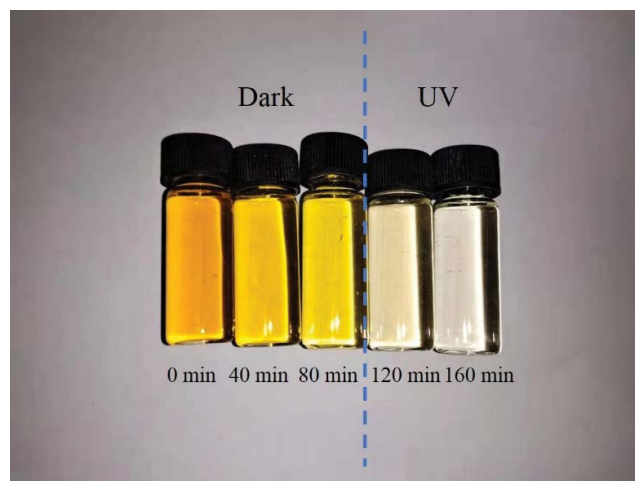


Fig. 13. Real degradation effect.

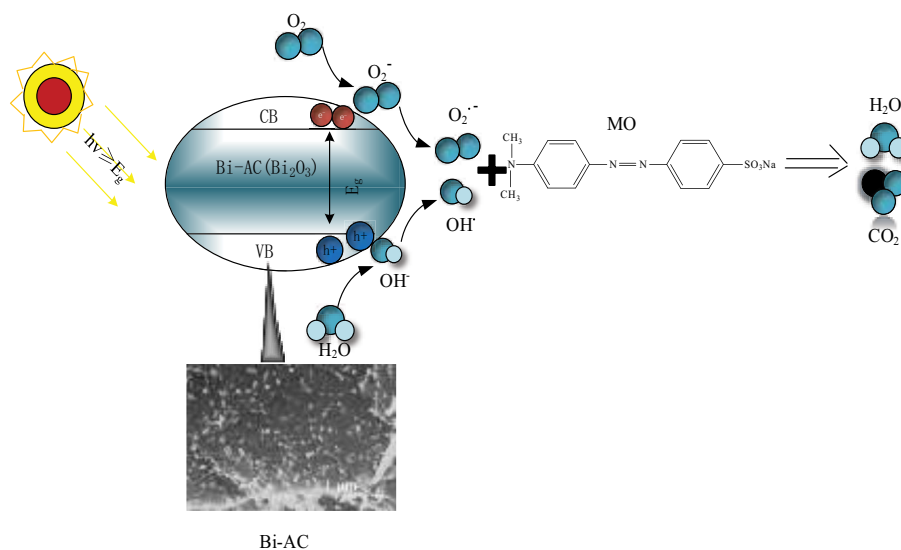


Fig. 14. Photocatalysis mechanism diagram.

Table 6

Removal effect of Bi-AC repeated use (dose = 50 mg; volume = 200 mL; contact time = 120 min)

Number of uses	1	2	3	4	5
Removal rate	91.65%	89.78%	88.11%	86.75%	86.15%

was degraded under light irradiation in the second step. The photons in Bi_2O_3 were excited and the electrons were excited to pass through the forbidden band (E_g) to the conduction band (CB) to form photogenerated electrons (e^-) so formed the corresponded valence band (VB) in the light condition as shown in Fig. 14. Then the photogenerated electron (e^-) and the hole pair (h^+) migrate to the Bi-AC surface. O_2 adsorbed on the surface of Bi-AC was trapped by highly reducing photogenerated electrons (e^-) producing superoxide ion radicals (O_2^-). H_2O and hole pairs (h^+) produces hydroxyl radicals (OH^*). O_2^- and OH^* had strong oxidizing properties which could degrade MO in wastewater into H_2O , CO_2 and small inorganic molecules [40–42].

3.4.3. Reuse of Bi-AC

Table 6 reveals that the removal rate of Bi-AC to degrade the MO solution by under ultraviolet light

irradiation for five cycles. In this experiment, weighed 50 mg of Bi-AC for a concentration of 200 mg L^{-1} and a volume of 200 mL of MO in the dark for 80 min to remove the effect of adsorption. From Table 6 it can be seen that the removal rate of primary use was higher due to the higher activity. After the first recovery, the removal rate decreased significantly. The reason for partial deactivation may be due to the dye molecules in the reaction covering the surface of the activated carbon resulting in a decrease in Bi-AC activity. It was also can be found that the performance of Bi-AC in the second recovery was not significantly different from that the first recovery which indicates that the activity of Bi-AC becomes more stable after some active sites were passivated in the photoreaction. The experiment proves that the removal rate could still be maintained above 86% after five cycles of use. So the Bi-AC could be recycled multiple times in order to reduce operating costs.

3.5. Comparison with other materials

To compare the photocatalytic performance of Bi-AC with other materials, the results are given in Table 7. As can be seen, the photocatalytic performance of Bi-AC were higher than other specified adsorbents. In this sense, it can be concluded that the Bi-AC can be considered a promising adsorbent for the removal of organic dye.

Table 7

Comparison for the removal of dyes by different catalyst

Catalyst	Dye	Dose (mg)	Initial concentration (mg L^{-1})	Removal efficiency
Ag-TiO ₂ -AC [43]	MO	10	20	97.4%
TiO ₂ /Cs-MT [44]	MO	10	20	95.8%
ZnO/Au@Cu ₂ O [45]	MO	10	20	93%
Mesoporous ZSM-5 [46]	MO	120	100	94.3%
Bi-AC	MO	50	200	94.9%

4. Conclusion

The Bi-AC was prepared by used the S-AC and Bi (NO₃)₃·5H₂O as raw material under dipped-microwave roasted. In this study, the Bi-AC roasted at 900°C using the heats time of 20 min can be gained the optimal experimental condition, the maximum MB adsorption value of Bi-AC is 210 mg L⁻¹. The adsorption performance of Bi-AC was better than R-AC in this condition. The adsorption isotherm studies indicated that adsorption followed Langmuir isotherm, the maximum adsorption capacity of Bi-AC for MO can reach 352.5 mg g⁻¹. The kinetic results revealed that the adsorption process of Bi-AC and R-AC followed pseudo-second-order. The prepared Bi-AC exhibited excellent photocatalytic performance toward MO solution, with a removal efficiency of 94.9% under UV light irradiation. Moreover, the Bi-AC displayed excellent reusability. The experiment proves that the removal rate could still be maintained above 86% after five cycles of use. The results shown that the prepared Bi-AC is a new type of material combined with adsorption-photocatalysis which can effectively degrade dye wastewater.

Acknowledgements

Financial aid from the following programs is gratefully acknowledged: National Natural Science Foundation of China (51522405), Yunnan Ten Thousand Talents Plan Industrial Technology Talents Project (2019–1096), Yunnan Ten Thousand Talents Plan Young & Elite Talents Project (2018–73).

References

- X. Jiang, H.Y. Xia, L.B. Zhang, J.H. Peng, S. Cheng, Q. Zhang, Preparation of copper loaded activated carbon by ultrasound-microwave combined treating on waste activated carbon, *Powder Technol.*, 338 (2018) 857–868.
- S. Cheng, L.B. Zhang, H.Y. Xia, J.H. Peng, J.H. Shu, C.Y. Li, Adsorption behavior of methylene blue onto waste-derived adsorbent and exhaust gases recycling, *RSC Adv.*, 44 (2017) 27331–27341.
- A. Nasrollahpour, S.E. Moradi, Photochemical degradation of methylene blue by metal oxide-supported activated carbon photocatalyst, *Desal. Water Treat.*, 57 (2016) 8854–8862.
- Secretariat of China Dyestuff Industry Association, Analysis of the Economic Operation of China's Dyed Pigment Industry in 2017, *Fine and Specialty Chemicals*, 26 (2018) 5–13.
- J.G. Georgiadis, B.J. Marinas, A.M. Mayes, M.A. Shannon, P.W. Bohn, Science and technology for water purification in the coming decades, *Nature.*, 452 (2008) 301–310.
- M.R. Hoffmann, S.T. Martin, W. Choi, D.W. Bahnemann, Environmental applications of semiconductor photocatalysis, *Chem. Rev.*, 95 (1995) 69–96.
- J. Hou, C. Yang, Z. Wang, W. Zhou, S. Jiao, H. Zhu, In situ synthesis of α - β phase heterojunction on Bi₂O₃ nanowires with exceptional visible-light photocatalytic performance, *Appl. Catal., B*, 142–143 (2013) 504–511.
- S. Cotillas, J. Llanos, D.P.C. Clematis, M. Panizza, Removal of Procion Red MX-5B dye from wastewater by conductive-diamond electrochemical oxidation, *Electrochim. Acta*, 263 (2018) 1–7.
- Y. Huang, G. Ruan, Y. Ruan, W. Zhang, X. Li, F. Du, J. Li, Hypercrosslinked porous polymers hybridized with graphene oxide for water treatment: dye adsorption and degradation, *RSC Adv.*, 8 (2018) 13417–13422.
- A.K. Verma, R.R. Dash, P. Bhunia, A review on chemical/flocculation technologies for removal of colour from textile wastewaters, *J. Environ. Manage.*, 93 (2012) 154–168.
- A.E.D.F. Marcela, B.D.C. Cassandra, M.M. Bonetto, D.P.S. Rafael, L.A. Féris, Diclofenac removal from water by adsorption using activated carbon in batch mode and fixed-bed column: isotherms, thermodynamic study and breakthrough curves modeling, *J. Cleaner Prod.*, 181 (2018) 145–154.
- B.-T. Zhang, H. Liu, Y. Liu, Y.G. Teng, Application trends of nanofibers in analytical chemistry, *TrAC, Trends Anal. Chem.*, 131 (2020) 115992, doi: 10.1016/j.trac.2020.115992.
- L. Pan, Y. Takagi, Y. Matsui, T. Matsushita, N. Shirasaki, Micro-milling of spent granular activated carbon for its possible reuse as an adsorbent: remaining capacity and characteristics, *Water Res.*, 114 (2017) 50–58.
- T.S. Kim, H.J. Song, M.A. Dar, H.J. Lee, D.W. Kim, Fast adsorption kinetics of highly dispersed ultrafine nickel/carbon nanoparticles for organic dye removal, *Appl. Surf. Sci.*, 439 (2018) 364–370.
- A. Fujishima, K. Honda, Electrochemical photolysis of water at a semiconductor electrode, *Nature*, 238 (1972) 37–38.
- J. Li, J. Zhong, X. He, S. Huang, J. Zeng, J. He, W. Shi, Enhanced photocatalytic activity of Fe₂O₃ decorated Bi₂O₃, *Appl. Surf. Sci.*, 284 (2013) 527–532.
- J. Zhong, J. Li, J. Zeng, J. He, S. Huang, W. Jiang, M. Li, Enhanced photocatalytic activity of In₂O₃-decorated TiO₂, *Appl. Phys. A*, 115 (2014) 1231–1238.
- P. Cai, S.M. Zhou, D.K. Ma, S.N. Liu, W. Chen, S.M. Huang, Fe₂O₃-modified porous BiVO₄ nanoplates with enhanced photocatalytic activity, *Nano-Micro. Lett.*, 7 (2015) 183–193.
- J.Z. Li, J.B. Zhong, J. Zeng, F.M. Feng, J.J. He, Improved photocatalytic activity of dysprosium-doped Bi₂O₃ prepared by sol-gel method, *Mater. Sci. Semicond. Process.*, 16 (2013) 379–384.
- Y. Dai, L. Yin, Low Fe-doped Bi₂O₃ photocatalyst with long wavelength response: crystalline transition and mechanisms by first-principles calculation, *J. Alloys Compd.*, 563 (2013) 80–84.
- N. Xia, D. Yuan, T. Zhou, J. Chen, S. Mo, Y. Liu, Microwave synthesis and electrochemical characterization of mesoporous carbon@Bi₂O₃ composites, *Mater. Res. Bull.*, 46 (2011) 687–691.
- M. Malligavathy, D.P. Padiyan, Phase purity analysis and optical studies of Bi₂O₃ nanoparticles suitable for photocatalytic activity, *Int. J. Nanomed.*, 17 (2018) 1760040, doi: 10.1142/S0219581X17600407.
- S.A. Hosseini, R. Saeedi, Photocatalytic degradation of methyl orange on Bi₂O₃ and Ag₂O-Bi₂O₃ nano photocatalysts, *Bull. Chem. React. Eng. Catal.*, 12 (2017) 96, doi: 10.9767/brec.12.1.623.96-105.
- X. Liu, X. Quan, L. Bo, S. Chen, Y. Zhao, M. Chang, Temperature measurement of GAC and decomposition of PCP loaded on GAC and GAC-supported copper catalyst in microwave irradiation, *Appl. Catal., A*, 264 (2004) 53–58.
- P. Arabkhani, H. Javadian, A. Asfaram, M. Ateia, Decorating graphene oxide with zeolitic imidazolate framework (ZIF-8) and pseudo-boehmite offers ultra-high adsorption capacity of diclofenac in hospital effluents, *Chemosphere*, 271 (2021) 129610, doi: 10.1016/j.chemosphere.2021.129610.
- M. Asfaram, G. Ghaedi, R. Ghezl bash, Biosorption of malachite green by novel biosorbent *Yarrowia lipolytica* isf7: application of response surface methodology, *J. Mol. Liq.*, 214 (2016) 249–258.
- H. Abbasi, F. Salimi, F. Golmohammadi, Removal of cadmium from aqueous solution by nano composites of bentonite/TiO₂ and bentonite/ZnO using photocatalysis adsorption process, *Silicon-Neth. Silicon*, 12 (2020) 2721–2731.
- M. Kamari, S. Shafiee, F. Salimi, Comparison of modified boehmite nanoplatelets and nanowires for dye removal from aqueous solution, *Desal. Water Treat.*, 161 (2019) 304–314.
- J. Rezaee, F. Salimi, C. Karami, Removal of eriochrome black T dye from water solution using modified nano-boehmite by organic compounds, *Desal. Water Treat.*, 139 (2019) 342–351.
- P. Arabkhani, A. Asfaram, Development of a novel three-dimensional magnetic polymer aerogel as an efficient adsorbent for malachite green removal, *J. Hazard. Mater.*, 384 (2019) 121394, doi: 10.1016/j.jhazmat.2019.121394.
- M. Roosta, M. Ghaedi, A. Asfaram, Simultaneous ultrasonic-assisted removal of malachite green and safranin O by copper

- nanowires loaded on activated carbon: central composite design optimization, *RSC Adv.*, 5 (2015) 57021–57029.
- [32] Q. Huang, S. Zhang, C. Cai, B. Zhou, β - and α - Bi_2O_3 nanoparticles synthesized via microwave-assisted method and their photocatalytic activity towards the degradation of rhodamine B, *Mater. Lett.*, 65 (2011) 988–990.
- [33] J.Y. Liu, Preparation of Cerium Oxide Composite and its Application in Photocatalysis, Ph.D. Dissertation, East China Normal University, Shanghai, 2015 (in Chinese).
- [34] H. Sudrajat, S. Hartuti, Structural properties and catalytic activity of a novel ternary $\text{CuO/g-C}_3\text{N}_4/\text{Bi}_2\text{O}_3$ photocatalyst, *J. Colloid Interface Sci.*, 524 (2018) 227–235.
- [35] H. Jiang, C. Wang, P. Wang, J. Li, Z. Lu, Surface properties and visible-light photocatalytic activity of N-doped TiO_2 nano-powder, *J. Mater. Sci. Eng.*, 29 (2011) 161–166.
- [36] M. Wang, Q. Liu, Y. Che, L. Zhang, D. Zhang, Characterization and photocatalytic properties of N-doped BiVO_4 synthesized via sol-gel method, *J. Alloys Compd.*, 548 (2013) 70–76.
- [37] Y. Shi, L. Luo, Y. Zhang, Y. Chen, S. Wang, L. Li, F. Jiang, Synthesis and characterization of α/β - Bi_2O_3 with enhanced photocatalytic activity for 17 α -ethynylestradiol, *Ceram. Int.*, 43 (2017) 7267–7635.
- [38] K.S. Novoselov, V.I. Falko, L. Colombo, P.R. Gellert, M.G. Schwab, K. Kim, A roadmap for grapheme, *Nature*, 490 (2012) 192–200.
- [39] F. Salimi, V. Valiei, C. Karami, Removal of EBT dye from aqueous solution by modified MoNiO_4 adsorbent. *Desal. Water Treat.*, 190 (2020) 340–352.
- [40] M. Jalalah, M. Faisal, H. Bouzid, J.G. Park, S.A.A. Sayari, A.A. Ismail, Comparative study on photocatalytic performances of crystalline α - and β - Bi_2O_3 nanoparticles under visible light, *J. Ind. Eng. Chem.*, 309 (2015) 183–189.
- [41] G. Dai, S. Liu, Y. Liang, A simple preparation of carbon doped porous Bi_2O_3 with enhanced visible-light photocatalytic activity, *J. Alloys Compd.*, 608 (2014) 44–48.
- [42] S. Chen, J. Zhang, C. Zhang, Q. Yue, Y. Li, C. Li, Equilibrium and kinetic studies of methyl orange and methyl violet adsorption on activated carbon derived from *Phragmites australis*, *Desalination*, 252 (2010) 149–156.
- [43] R. Shan, L. Lu, J. Gu, Y. Zhang, H. Yuan, Y. Chen, B. Luo, Photocatalytic degradation of methyl orange by $\text{Ag}/\text{TiO}_2/\text{biochar}$ composite catalysts in aqueous solutions, *Mater. Sci. Semicond. Process.*, 114 (2020) 105088, doi: 10.1016/j.mssp.2020.105088.
- [44] N.N. Bahrudin, M. Nawi, Z. Zainal, Insight into the synergistic photocatalytic-adsorptive removal of methyl orange dye using $\text{TiO}_2/\text{chitosan}$ based photocatalyst, *Int. J. Biol. Macromol.*, 165 (2020) 2462–2474.
- [45] X. Yuan, F. Pei, X. Luo, H. Hu, H. Qian, P. Wen, K. Miao, S. Guo, W. Wang, G. Feng, Fabrication of $\text{ZnO}/\text{Au}/\text{Cu}_2\text{O}$ heterojunction towards deeply oxidative photodegradation of organic dyes, *Sep. Purif. Technol.*, 262 (2021) 118301, doi: 10.1016/j.seppur.2021.118301.
- [46] S. Radoor, J. Karayil, A. Jayakumar, J. Parameswaranpillai, S. Siengchin, Efficient removal of methyl orange from aqueous solution using mesoporous ZSM-5 zeolite: synthesis, kinetics and isotherm studies, *Colloids Surf., A*, 611 (2021) 125852, doi: 10.1016/j.colsurfa.2020.125852.